Chapter 12
Gravitational Waves

Gravitational waves are a hot topic today. It is now possible to directly detect gravitational waves from astrophysical sources, and we expect an impressive amount of completely new data in the next 10–20 years. The aim of this chapter is to provide an introductory overview on the topic. Contrary to the other chapters of the book, the discussion will not be at a purely theoretical level, and some sections will be devoted to observations and experimental facilities.

12.1 Historical Overview

Generally speaking, gravitational waves should be a prediction of any relativistic theory of gravity. Matter makes the spacetime curved, and therefore the motion of matter can alter the spacetime metric. Gravitational waves are like "ripples" in the curvature of the spacetime propagating at a finite velocity. Consistently with the Einstein Principle of Relativity, no signal can propagate (locally) at a velocity higher than the speed of light in vacuum.

Gravitational waves were predicted by Albert Einstein immediately after the formulation of his theory. However, the gravitational wave signal produced by typical astrophysical sources is extremely weak, and therefore the detection of gravitational waves is very challenging.

The first observational evidence for the existence of gravitational waves followed the discovery of the binary pulsar PSR 1913+16 by Russell Alan Hulse and Joseph Hooton Taylor in 1974. PSR 1913+16 is a binary system of two neutron stars, and one of them is seen as a pulsar, which makes this system a perfect laboratory for testing the predictions of Einstein's gravity. Since its discovery, the orbital period of PSR 1913+16 has decayed in agreement with the predictions of Einstein's equations for the emission of gravitational waves. From the radio data covering about 40 years of observations, we have [13]

C. Bambi, *Introduction to General Relativity*, Undergraduate Lecture Notes in Physics, https://doi.org/10.1007/978-981-13-1090-4_12

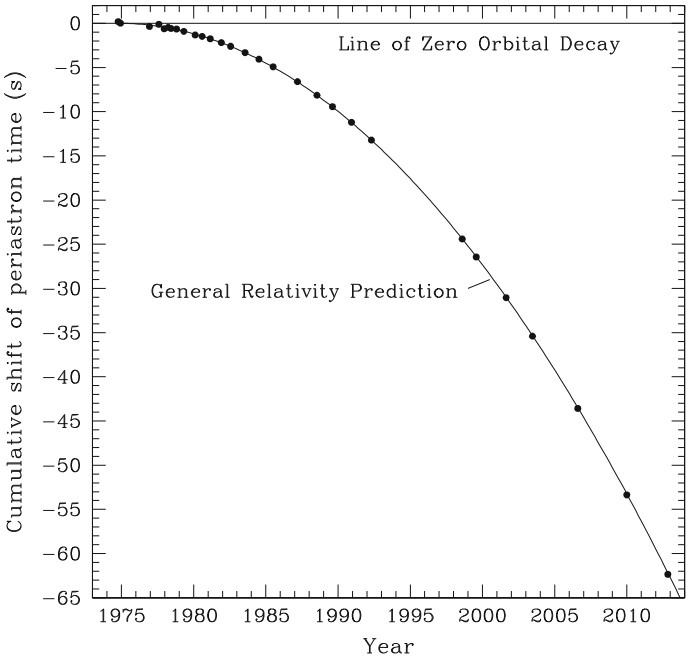

Fig. 12.1 Cumulative shift of the periastron time of PSR 1913+16 over about 40 years, from 1974 to 2012. The dots (with error bars too small to show) are the data and the solid curve is the prediction of Einstein's gravity for the emission of gravitational waves. From [13]. ©AAS. Reproduced with permission

$$\frac{\dot{P}_{\text{corrected}}}{\dot{P}_{\text{GR}}} = 0.9983 \pm 0.0016\,, \tag{12.1}$$

where $\dot{P}_{\text{corrected}}$ is the (corrected) observed orbital decay[1] and $\dot{P}_{\text{GR}}$ is the orbital decay due to gravitational waves expected in Einstein's gravity. Figure 12.1 shows the perfect agreement between the data (the black dots) and the theoretical prediction (the solid line).

Attempts of direct detection of gravitational waves started in the 1960s, with the resonant bar constructed by Joseph Weber. It was a 2 m aluminum cylinder held at room temperature and isolated from vibrations in a vacuum chamber. In the 1990s, a new generation of resonant detectors became operative, as well as the first generation of laser interferometers.

The first direct detection of gravitational waves was announced by the LIGO-Virgo collaboration in February 2016 [1]. The event, called GW150914 because it was detected on 14 September 2015, was the coalescence of two stellar-mass black

[1] One has to remove the effect due to the relative acceleration between us and the pulsar caused by the differential rotation of the Galaxy.

holes, both of about 30 $M_\odot$. They formed a black hole of about 60 $M_\odot$, releasing an energy of about 3 $M_\odot$ in the form of gravitational waves.

12.2 Gravitational Waves in Linearized Gravity

Let us consider a spacetime where we can write, not necessarily over the whole spacetime but at least on a sufficiently large region, the metric $g_{\mu\nu}$ as the Minkowski metric $\eta_{\mu\nu}$ plus a small perturbation $h_{\mu\nu}$

$$g_{\mu\nu} = \eta_{\mu\nu} + h_{\mu\nu}\,, \quad |h_{\mu\nu}| \ll 1\,. \tag{12.2}$$

$h_{\mu\nu}$ is called the *metric perturbation*. In linearized gravity, we neglect terms of second or higher order in $h_{\mu\nu}$. Indices of "tensors" of order $h_{\mu\nu}$ are raised and lowered using the Minkowski metric $\eta_{\mu\nu}$. The inverse metric $g^{\mu\nu}$ is

$$g^{\mu\nu} = \eta^{\mu\nu} - h^{\mu\nu} \tag{12.3}$$

Indeed, if we write $g^{\mu\nu} = \eta^{\mu\nu} + H^{\mu\nu}$, we see that

$$\begin{aligned} g_{\mu\nu}g^{\nu\rho} &= \left(\eta_{\mu\nu} + h_{\mu\nu}\right)\left(\eta^{\nu\rho} + H^{\nu\rho}\right) \\ &= \eta^\rho_\mu + h^\rho_\mu + H^\rho_\mu + O\left(h^2\right)\,, \end{aligned} \tag{12.4}$$

and therefore $H^{\mu\nu} = -h^{\mu\nu}$. Note that $h_{\mu\nu}$ transforms as a tensor only under Lorentz transformations, but not under general coordinate transformations [see later Eqs. (12.18) and (12.19)].

Let us now write the Einstein equations in linearized gravity. From Eq. (5.76), the Riemann tensor $R_{\mu\nu\rho\sigma}$ is given by

$$R_{\mu\nu\rho\sigma} = \frac{1}{2}\left(\partial_\nu\partial_\rho h_{\mu\sigma} + \partial_\mu\partial_\sigma h_{\nu\rho} - \partial_\nu\partial_\sigma h_{\mu\rho} - \partial_\mu\partial_\rho h_{\nu\sigma}\right)\,. \tag{12.5}$$

The Ricci tensor is

$$\begin{aligned} R_{\nu\sigma} &= g^{\mu\rho}R_{\mu\nu\rho\sigma} = \eta^{\mu\rho}R_{\mu\nu\rho\sigma} \\ &= \frac{1}{2}\left(\partial_\nu\partial^\mu h_{\mu\sigma} + \partial^\rho\partial_\sigma h_{\nu\rho} - \partial_\nu\partial_\sigma h - \Box_\eta h_{\nu\sigma}\right) \end{aligned} \tag{12.6}$$

where $h = \eta^{\mu\nu}h_{\mu\nu}$ is the trace of the metric perturbation and $\Box_\eta = \eta^{\mu\nu}\partial_\mu\partial_\nu$ is the d'Alembertian of flat spacetime. Lastly, the scalar curvature is

$$\begin{aligned} R &= g^{\nu\sigma}R_{\nu\sigma} = \frac{1}{2}\left(\partial^\sigma\partial^\mu h_{\mu\sigma} + \partial^\rho\partial^\nu h_{\nu\rho} - \Box_\eta h - \Box_\eta h\right) \\ &= \partial^\mu\partial^\nu h_{\mu\nu} - \Box_\eta h\,. \end{aligned} \tag{12.7}$$

With Eqs. (12.6) and (12.7) we can write the Einstein equations

$$\frac{1}{2}\left(\partial_\mu\partial^\sigma h_{\sigma\nu} + \partial^\sigma\partial_\nu h_{\mu\sigma} - \partial_\mu\partial_\nu h - \Box_\eta h_{\mu\nu}\right) \\ -\frac{1}{2}\eta_{\mu\nu}\left(\partial^\sigma\partial^\rho h_{\sigma\rho} - \Box_\eta h\right) = \frac{8\pi G_\mathrm{N}}{c^4}T_{\mu\nu}\,. \tag{12.8}$$

Let us now simplify Eq. (12.8) by changing variables and coordinate system. First, we change variables. We define the *trace-reversed perturbation* as

$$\tilde{h}_{\mu\nu} = h_{\mu\nu} - \frac{1}{2}\eta_{\mu\nu}h\,. \tag{12.9}$$

The trace of $\tilde{h}_{\mu\nu}$ is

$$\tilde{h} = \eta^{\mu\nu}\tilde{h}_{\mu\nu} = \eta^{\mu\nu}\left(h_{\mu\nu} - \frac{1}{2}\eta_{\mu\nu}h\right) = h - 2h = -h\,, \tag{12.10}$$

and hence the name "trace-reversed". Note that

$$h_{\mu\nu} = \tilde{h}_{\mu\nu} - \frac{1}{2}\eta_{\mu\nu}\tilde{h}\,, \tag{12.11}$$

If we plug the expression (12.11) into Eq. (12.8), we find

$$\frac{1}{2}\left(\partial_\mu\partial^\sigma\tilde{h}_{\sigma\nu} - \frac{1}{2}\partial_\mu\partial_\nu\tilde{h} + \partial^\sigma\partial_\nu\tilde{h}_{\mu\sigma} - \frac{1}{2}\partial_\mu\partial_\nu\tilde{h} + \partial_\mu\partial_\nu\tilde{h} - \Box_\eta\tilde{h}_{\mu\nu} + \frac{1}{2}\eta_{\mu\nu}\Box_\eta\tilde{h}\right) \\ -\frac{1}{2}\eta_{\mu\nu}\left(\partial^\sigma\partial^\rho\tilde{h}_{\sigma\rho} - \frac{1}{2}\Box_\eta\tilde{h} + \Box_\eta\tilde{h}\right) = \frac{8\pi G_\mathrm{N}}{c^4}T_{\mu\nu}\,, \tag{12.12}$$

and the Einstein equations in linearized gravity in terms of the trace-reversed perturbation are

$$\partial_\mu\partial^\sigma\tilde{h}_{\sigma\nu} + \partial^\sigma\partial_\nu\tilde{h}_{\mu\sigma} - \Box_\eta\tilde{h}_{\mu\nu} - \eta_{\mu\nu}\partial^\sigma\partial^\rho\tilde{h}_{\sigma\rho} = \frac{16\pi G_\mathrm{N}}{c^4}T_{\mu\nu}\,. \tag{12.13}$$

12.2.1 Harmonic Gauge

Now we change coordinate system. We choose the coordinate system $\{x^\mu\}$ such that

$$\partial^\mu\tilde{h}_{\mu\nu} = 0\,. \tag{12.14}$$

The condition (12.14) is called the *harmonic gauge* (or the Hilbert gauge or the de Donder gauge). The choice of the harmonic gauge is similar to the choice of the

Lorentz gauge in Maxwell's theory, $\partial_\mu A^\mu = 0$ (see Chap. 4). In the harmonic gauge, Eq. (12.13) becomes

$$\Box_\eta \tilde{h}_{\mu\nu} = -\frac{16\pi G_{\rm N}}{c^4} T_{\mu\nu} \,. \tag{12.15}$$

It is easy to see that we can always choose the harmonic gauge. Let us consider the coordinate transformation

$$x^\mu \to x'^\mu = x^\mu + \xi^\mu \,, \tag{12.16}$$

where ξ^μs are four functions of x^μ of the same order as $h_{\mu\nu}$. The inverse is

$$x^\mu = x'^\mu - \xi^\mu \,, \tag{12.17}$$

and the spacetime metrics in the two coordinates systems are related by

$$\begin{aligned} g_{\mu\nu} \to g'_{\mu\nu} &= \frac{\partial x^\alpha}{\partial x'^\mu} \frac{\partial x^\beta}{\partial x'^\nu} g_{\alpha\beta} \\ &= \left(\delta^\alpha_\mu - \partial_\mu \xi^\alpha\right) \left(\delta^\beta_\nu - \partial_\nu \xi^\beta\right) \left(\eta_{\alpha\beta} + h_{\alpha\beta}\right) \\ &= \eta_{\mu\nu} + h_{\mu\nu} - \partial_\mu \xi_\nu - \partial_\nu \xi_\mu \,. \end{aligned} \tag{12.18}$$

Since $g'_{\mu\nu} = \eta_{\mu\nu} + h'_{\mu\nu}$, the relation between the two metric perturbations is

$$h'_{\mu\nu} = h_{\mu\nu} - \partial_\mu \xi_\nu - \partial_\nu \xi_\mu \,, \tag{12.19}$$

and we see that $h_{\mu\nu}$ does not transform as a tensor under general coordinate transformations.[2] The relation between the two trace-reversed perturbations is

$$\tilde{h}'_{\mu\nu} = h'_{\mu\nu} - \frac{1}{2}\eta_{\mu\nu} h' = \tilde{h}_{\mu\nu} - \partial_\mu \xi_\nu - \partial_\nu \xi_\mu + \eta_{\mu\nu} \partial^\sigma \xi_\sigma \,. \tag{12.21}$$

If we are not in the harmonic gauge, we can perform the coordinate transformation in (12.16) to have $\partial^\mu \tilde{h}'_{\mu\nu} = 0$

$$\partial^\mu \tilde{h}'_{\mu\nu} = \partial^\mu \tilde{h}_{\mu\nu} - \Box_\eta \xi_\nu = 0 \,, \tag{12.22}$$

and therefore we need ξ_ν such that

---

[2] $h_{\mu\nu}$ transforms as a tensor under Lorentz transformations. If the transformation is $x^\mu \to x'^\mu = \Lambda^\mu_\nu x^\nu$, we have

$$g_{\mu\nu} = \eta_{\mu\nu} + h_{\mu\nu} \to g'_{\mu\nu} = \Lambda^\alpha_\mu \Lambda^\beta_\nu \left(\eta_{\alpha\beta} + h_{\alpha\beta}\right) = \eta_{\mu\nu} + \Lambda^\alpha_\mu \Lambda^\beta_\nu h_{\alpha\beta} \,, \tag{12.20}$$

and we see that $h'_{\mu\nu} = \Lambda^\alpha_\mu \Lambda^\beta_\nu h_{\alpha\beta}$.

$$\Box_\eta \xi_\nu = \partial^\mu \tilde{h}_{\mu\nu} \,. \tag{12.23}$$

Note that if we are in the harmonic gauge and we consider a new transformation such that $\Box_\eta \xi_\mu = 0$, we remain in the harmonic gauge. This is the counterpart of the transformation $A_\mu \to A_\mu + \partial_\mu \Lambda$ in Maxwell's theory, where the Lorentz gauge is preserved if $\Box_\eta \Lambda = 0$.

The formal solution of Eq. (12.15) is

$$\tilde{h}_{\mu\nu}(t, \mathbf{x}) = \frac{4G_\mathrm{N}}{c^4} \int d^3\mathbf{x}' \frac{T_{\mu\nu}\left(t - |\mathbf{x} - \mathbf{x}'|/c, \mathbf{x}'\right)}{|\mathbf{x} - \mathbf{x}'|} \,, \tag{12.24}$$

where the integral is performed in the flat 3-dimensional space and $|\mathbf{x} - \mathbf{x}'|$ is the Euclidean distance between the point $\mathbf{x}$ and the point $\mathbf{x}'$. In Cartesian coordinates (x, y, z), we have

$$|\mathbf{x} - \mathbf{x}'| = \sqrt{(x - x')^2 + (y - y')^2 + (z - z')^2} \,. \tag{12.25}$$

12.2.2 Transverse-Traceless Gauge

$\tilde{h}_{\mu\nu}$ is symmetric and therefore has ten independent components. The harmonic gauge (12.14) provides four conditions and reduces the number of independent components to six. However, we still have the freedom to choose four arbitrary functions ξ_μ satisfying the equation $\Box_\eta \xi^\mu = 0$.

First, we can choose ξ^0 such that the trace of $\tilde{h}_{\mu\nu}$ vanishes, i.e. $\tilde{h} = 0$. Note that such a choice implies that the trace-reversed perturbation $\tilde{h}_{\mu\nu}$ and the metric perturbation $h_{\mu\nu}$ coincide

$$h_{\mu\nu} = \tilde{h}_{\mu\nu} \,, \tag{12.26}$$

and in what follows we can omit the tilde for simplicity when we are in this case. Second, we can choose the three functions ξ^is such that $h^{0i} = 0$.

Imposing $h^{0i} = 0$, the harmonic gauge condition (12.14) becomes

$$\partial^0 h_{00} = 0 \,, \tag{12.27}$$

namely h_{00} is independent of time and therefore corresponds to the Newtonian potential of the source. Restricting the attention to gravitational waves (i.e. the time-dependent part of h_{00}), we can set $h_{00} = 0$. Eventually we have

$$h_{0\mu} = 0 \,, \quad h = 0 \,, \quad \partial^i h_{ij} = 0 \,, \tag{12.28}$$

which defines the *transverse-traceless gauge* (TT gauge). Quantities in the TT gauge are often indicated with TT, e.g. $h^{\rm TT}_{\mu\nu}$.

Note that the TT gauge is only possible in vacuum, namely when Eq. (12.15) reads

$$\Box_\eta \tilde{h}_{\mu\nu} = 0\,. \tag{12.29}$$

Inside a source we can choose the harmonic gauge and we still have the freedom to choose the four functions ξ_μs satisfying the equation $\Box_\eta \xi_\mu = 0$. However, we cannot set to zero any further component of $\tilde{h}_{\mu\nu}$ by choosing suitable ξ_μs because $\Box_\eta \tilde{h}_{\mu\nu} \neq 0$.

The vacuum equation $\Box_\eta h^{\rm TT}_{\mu\nu} = 0$ has plane wave solutions ($h^{\rm TT}_{0\mu} = 0$ because we are in the TT gauge)

$$h^{\rm TT}_{ij} = \varepsilon_{ij} e^{ik^\mu x_\mu}\,, \tag{12.30}$$

where $k^\mu = (\omega/c, \mathbf{k})$, $\omega = |\mathbf{k}|c$ is the angular frequency of the gravitational wave, and ε_{ij} is the polarization tensor. For a gravitational wave propagating along the z direction, we have (ignoring the imaginary part and imposing that h_{ij} is symmetric and traceless)

$$h^{\rm TT}_{\mu\nu} = \begin{pmatrix} 0 & 0 & 0 & 0 \\ 0 & h_+ & h_\times & 0 \\ 0 & h_\times & -h_+ & 0 \\ 0 & 0 & 0 & 0 \end{pmatrix} \cos\left[\omega\,(t - z/c)\right]\,, \tag{12.31}$$

where h_+ and $h_\times$ are the amplitudes of the gravitational wave in the two polarizations. The ij components of $h^{\rm TT}_{\mu\nu}$ can be written as

$$h^{\rm TT}_{ij} = h_+ \varepsilon^+_{ij} \cos\left[\omega\,(t - z/c)\right] + h_\times \varepsilon^\times_{ij} \cos\left[\omega\,(t - z/c)\right] \tag{12.32}$$

where

$$\begin{aligned} \varepsilon^+_{ij} &= \begin{pmatrix} 1 & 0 & 0 \\ 0 & -1 & 0 \\ 0 & 0 & 0 \end{pmatrix} \qquad \text{(plus mode)}\,, \\ \varepsilon^\times_{ij} &= \begin{pmatrix} 0 & 1 & 0 \\ 1 & 0 & 0 \\ 0 & 0 & 0 \end{pmatrix} \qquad \text{(cross mode)}\,. \end{aligned} \tag{12.33}$$

With the metric perturbation (12.31), the line element reads

$$\begin{aligned} ds^2 = &-c^2 dt^2 + (1 + h_+ \cos\phi)\, dx^2 + (1 - h_+ \cos\phi)\, dy^2 \\ &+ 2h_\times \cos\phi\, dx dy + dz^2\,, \end{aligned} \tag{12.34}$$

where $\phi = \omega\,(t - z/c)$.

Let us now check the effect of the gravitational wave in (12.34) on a free point-like particle. The particle is at rest at $\tau = 0$. The geodesic equations of the particle at $\tau = 0$ read

$$\left(\ddot{x}^i + \Gamma^i_{00}\dot{x}^0\dot{x}^0\right)_{\tau=0} = 0\,, \tag{12.35}$$

because $\dot{x}^i = 0$ at $\tau = 0$. Γ^i_{00} is

$$\begin{aligned}\Gamma^i_{00} &= \frac{1}{2}\eta^{i\mu}\left(\partial_0 h_{\mu 0} + \partial_0 h_{0\mu} - \partial_\mu h_{00}\right)\\ &= \partial_0 h^i_0 - \frac{1}{2}\partial^i h_{00}\,,\end{aligned} \tag{12.36}$$

and in the TT gauge vanishes, $\Gamma^i_{00} = 0$. This means that $\ddot{x}^i = 0$, and therefore $\dot{x}^i = 0$ at all times and the particle remains at rest. This result should not be interpreted as the passage of gravitational waves having no physical effects, because in general relativity the choice of the coordinate system is arbitrary. In fact, the opposite is true, namely that the coordinates do not have a direct physical meaning.

Let us now consider two free point-like particles at rest, respectively with space coordinates $(x_0, 0, 0)$ and $(-x_0, 0, 0)$. The proper distance between the two particles is

$$\begin{aligned}L(t) &= \int_{-x_0}^{x_0}\sqrt{g_{xx}}dx' = \int_{-x_0}^{x_0}\sqrt{1 + h_{xx}}dx'\\ &\approx L_0\left[1 + \frac{1}{2}h_+\cos(\omega t)\right]\,,\end{aligned} \tag{12.37}$$

where $L_0 = 2x_0$ is their proper distance in the absence of gravitational waves. If the two particles have instead, respectively, coordinates $(0, x_0, 0)$ and $(0, -x_0, 0)$, we find

$$L(t) \approx L_0\left[1 - \frac{1}{2}h_+\cos(\omega t)\right]\,. \tag{12.38}$$

We thus see that the proper distance between the two particles changes with time periodically and the variation is proportional to the amplitude of the gravitational wave. If we consider a rotation of 45° in the xy plane, we find the expressions in Eqs. (12.37) and (12.38) with h_+ replaced by $h_\times$. In the end, it is easy to see that the passage of a gravitational wave propagating along the z direction on a ring of particles in the xy-plane is that illustrated in Fig. 12.2.

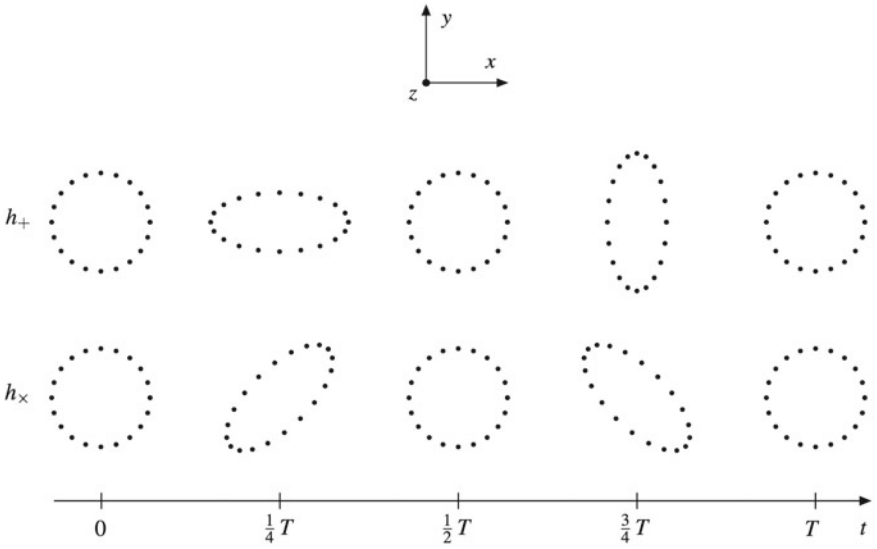

Fig. 12.2 Impact of a gravitational wave traveling along the z-axis on a ring of test-particles in the xy-plane. The effect of the polarization modes h_+ and $h_\times$ is the same modulo a rotation of 45° on the xy-plane. $T = 2\pi/\omega$ is the period of the gravitational wave

12.3 Quadrupole Formula

If we can assume that the region where the source is confined (i.e. $T^{\mu\nu}$ is non-vanishing) is much smaller than the wavelength of the emitted radiation, Eq. (12.24) can be approximated as

$$\tilde{h}^{\mu\nu}(t, \mathbf{x}) = \frac{4G_{\mathrm{N}}}{c^4 r} \int d^3\mathbf{x}' T^{\mu\nu}\left(t - r/c, \mathbf{x}'\right) , \tag{12.39}$$

where $r = |\mathbf{x}|$.

In the linearized theory, $h_{\mu\nu}$ and $T_{\mu\nu}$ are of the same order and therefore we have $\partial_\mu T^{\mu\nu} = 0$ with the partial derivative. We write $\partial_\mu T^{\mu\nu} = 0$ as $\partial_0 T^{0\nu} = -\partial_k T^{k\nu}$ and then we integrate over the volume V containing all of the region with $T_{\mu\nu} \neq 0$

$$\frac{1}{c}\frac{\partial}{\partial t}\int_V T^{0\nu}\, d^3\mathbf{x} = -\int_V \frac{\partial T^{k\nu}}{\partial x^k}\, d^3\mathbf{x} = -\int_\Sigma T^{k\nu}\, d\Sigma_k = 0 , \tag{12.40}$$

where Σ is the surface of the volume V and $T^{\mu\nu} = 0$ on Σ. We have thus

$$\int_V T^{0\nu}\, d^3\mathbf{x} = \text{constant} , \tag{12.41}$$

which implies $\tilde{h}^{0\nu}$ is constant too. Since here we are interested in gravitational waves, namely in the time-dependent part of the gravitational field, we can put $\tilde{h}^{0\nu} = 0$.

We write $\partial_\mu T^{\mu i} = 0$ as $\partial_0 T^{0i} = -\partial_k T^{ki}$, we multiply both sides by x^j, and we integrate over the volume V. We obtain

$$\begin{aligned}\frac{1}{c}\frac{\partial}{\partial t}\int_V T^{i0}x^j\,d^3\mathbf{x} &= -\int_V \frac{\partial T^{ik}}{\partial x^k}x^j\,d^3\mathbf{x}\\ &= -\int_V \frac{\partial}{\partial x^k}\left(T^{ik}x^j\right)d^3\mathbf{x} + \int_V T^{ik}\frac{\partial x^j}{\partial x^k}d^3\mathbf{x}\\ &= -\int_\Sigma T^{ik}x^j\,d\Sigma_k + \int_V T^{ij}d^3\mathbf{x}\\ &= \int_V T^{ij}d^3\mathbf{x}\,. \end{aligned} \tag{12.42}$$

Since $T^{\mu\nu}$ is a symmetric tensor, we can also write Eq. (12.42) by exchanging i and j and

$$\frac{1}{c}\frac{\partial}{\partial t}\int_V \left(T^{i0}x^j + T^{j0}x^i\right)d^3\mathbf{x} = 2\int_V T^{ij}d^3\mathbf{x}\,. \tag{12.43}$$

Let us now write $\partial_\mu T^{\mu 0} = 0$ as $\partial_0 T^{00} = -\partial_k T^{k0}$. This time we multiply both sides by $x^i x^j$. We integrate over the volume V and we find

$$\begin{aligned}\frac{1}{c}\frac{\partial}{\partial t}\int_V T^{00}x^i x^j\,d^3\mathbf{x} &= -\int_V \frac{\partial T^{k0}}{\partial x^k}x^i x^j\,d^3\mathbf{x}\\ &= -\int_V \frac{\partial}{\partial x^k}\left(T^{k0}x^i x^j\right)d^3\mathbf{x} + \int_V \left(T^{k0}\frac{\partial x^i}{\partial x^k}x^j + T^{k0}x^i\frac{\partial x^j}{\partial x^k}\right)d^3\mathbf{x}\\ &= -\int_\Sigma T^{k0}x^i x^j\,d\Sigma_k + \int_V \left(T^{i0}x^j + T^{j0}x^i\right)d^3\mathbf{x}\\ &= \int_V \left(T^{i0}x^j + T^{j0}x^i\right)d^3\mathbf{x}\,. \end{aligned} \tag{12.44}$$

We take a derivative with respect to the time t and we use Eq. (12.43)

$$\begin{aligned}\frac{1}{c^2}\frac{\partial^2}{\partial^2 t}\int_V T^{00}x^i x^j\,d^3\mathbf{x} &= \frac{1}{c}\frac{\partial}{\partial t}\int_V \left(T^{i0}x^j + T^{j0}x^i\right)d^3\mathbf{x}\\ &= 2\int_V T^{ij}d^3\mathbf{x}\,. \end{aligned} \tag{12.45}$$

We define the *quadrupole moment* of the source as

$$Q^{ij}(t) = \frac{1}{c^2}\int_V T^{00}(t,\mathbf{x})\,x^i x^j\,d^3\mathbf{x}\,. \tag{12.46}$$

Equation (12.39) becomes

$$\tilde{h}_{\mu 0} = 0\,,$$
$$\tilde{h}_{ij} = \frac{2G_{\rm N}}{c^4 r}\,\ddot{Q}_{ij}\,(t - r/c)\,, \tag{12.47}$$

where the double dot stands for the double derivative with respect to t and $\ddot{Q}_{ij}$ is evaluated at the time $t - r/c$. It is worth noting that a spherical or axisymmetric distribution of matter has a constant quadrupole moment, even if the body is rotating. This implies, for instance, that there is no emission of gravitational waves in a perfectly spherically symmetric collapse, in a perfectly axisymmetric rotating body, etc. Gravitational waves are emitted when there is a certain "degree of asymmetry", e.g. the coalescence of two objects, non-radial pulsation of a body, etc.

If we want Eq. (12.47) in the TT gauge, we need a coordinate transformation that preserves the harmonic gauge and switches to the TT gauge. This can be done with a projector operator. We already have $\tilde{h}_{\mu 0} = 0$. The traceless and transverse wave conditions read, respectively,

$$\delta^{ij} h^{\rm TT}_{ij} = 0\,, \quad n^i h^{\rm TT}_{ij} = 0\,, \tag{12.48}$$

where $\mathbf{n} = \mathbf{x}/r$ is the unit vector normal to the wavefront.

The operator to project a vector onto the plane orthogonal to the direction of $\mathbf{n}$ is

$$P_{ij} = \delta_{ij} - n_i n_j\,. \tag{12.49}$$

P_{ij} is symmetric and projects out any component parallel to $\mathbf{n}$:

$$P_{ij} n^i = \delta_{ij} n^i - n_i n_j n^i = n_j - n_j = 0\,. \tag{12.50}$$

The transverse-traceless projector is

$$P_{ijkl} = P_{ik} P_{jl} - \frac{1}{2} P_{ij} P_{kl}\,, \tag{12.51}$$

and extracts the transverse-traceless part of any tensor of type (0, 2). $h^{\rm TT}_{ij}$ is given by

$$h^{\rm TT}_{ij} = P_{ijkl} \tilde{h}_{kl}\,. \tag{12.52}$$

It is easy to check that the new tensor is traceless

$$\begin{aligned}
\delta^{ij} h^{\rm TT}_{ij} &= \delta^{ij} \left(P_{ik} P_{jl} - \frac{1}{2} P_{ij} P_{kl} \right) \tilde{h}_{kl} \\
&= \delta^{ij} \left[(\delta_{ik} - n_i n_k) \left(\delta_{jl} - n_j n_l \right) - \frac{1}{2} \left(\delta_{ij} - n_i n_j \right) (\delta_{kl} - n_k n_l) \right] \tilde{h}_{kl}
\end{aligned}$$

$$
\begin{aligned}
&= \delta^{ij}\left(\delta_{ik}\delta_{jl} - \delta_{ik}n_j n_l - \delta_{jl}n_i n_k + n_i n_k n_j n_l\right)\tilde{h}_{kl} \\
&\quad -\frac{1}{2}\delta^{ij}\left(\delta_{ij}\delta_{kl} - \delta_{ij}n_k n_l - \delta_{kl}n_i n_j + n_i n_j n_k n_l\right)\tilde{h}_{kl} \\
&= \tilde{h} - n_k n_l \tilde{h}_{kl} - \frac{1}{2}\left(3\tilde{h} - 3n_k n_l \tilde{h}_{kl} - \tilde{h} + n_k n_l \tilde{h}_{kl}\right) = 0\,. \qquad (12.53)
\end{aligned}
$$

Note that

$$
h_{ij}^{\mathrm{TT}} = P_{ijkl}h_{kl} = P_{ijkl}\tilde{h}_{kl}\,, \qquad (12.54)
$$

because h_{ij} and $\tilde{h}_{ij}$ only differ by the trace, which is projected out by P_{ijkl}.

Applying the projector P_{ijkl} to $\tilde{h}_{kl}$, Eq. (12.47) becomes

$$
\begin{aligned}
h_{\mu 0}^{\mathrm{TT}} &= 0\,, \\
h_{ij}^{\mathrm{TT}} &= \frac{2G_{\mathrm{N}}}{c^4 r}\ddot{Q}_{ij}^{\mathrm{TT}}\left(t - r/c\right)\,, \qquad (12.55)
\end{aligned}
$$

where

$$
Q_{ij}^{\mathrm{TT}} = P_{ijkl}Q_{kl}\,. \qquad (12.56)
$$

It is sometimes convenient to introduce the *reduced quadrupole moment*, which is defined as

$$
\tilde{Q}_{ij} = Q_{ij} - \frac{1}{3}\delta_{ij}Q\,, \qquad (12.57)
$$

where $Q = Q_i^i$ is the trace of the quadrupole moment. Note that

$$
Q_{ij}^{\mathrm{TT}} = P_{ijkl}\tilde{Q}_{kl} = P_{ijkl}Q_{kl}\,, \qquad (12.58)
$$

because Q_{ij} and $\tilde{Q}_{ij}$ only differ by the trace.

12.4 Energy of Gravitational Waves

Let us now evaluate the energy carried by a gravitational wave with the help of the pseudo-tensor of Landau–Lifshitz met in Sect. 7.5.

We consider a Cartesian coordinate system (x, y, z) in which the astrophysical source emitting gravitational waves is at the origin and the observer is far from the source with coordinates $(0, 0, z)$. The observer detects a gravitational wave traveling along the z axis. For simplicity, let us assume that the wave has only the plus polarization. The metric perturbation in the TT gauge reads

$$||h^{\mathrm{TT}}_{\mu\nu}|| = \begin{pmatrix} 0 & 0 & 0 & 0 \\ 0 & h_+(t,z) & 0 & 0 \\ 0 & 0 & -h_+(t,z) & 0 \\ 0 & 0 & 0 & 0 \end{pmatrix}, \tag{12.59}$$

where z is the z-coordinate of the observer. The amplitude of the gravitational wave h_+ has the form

$$h_+(t,z) = \frac{C\, f\,(t - z/c)}{z}\,. \tag{12.60}$$

where C and f are, respectively, a constant and a function that depends on the parameters and the nature of the emitting source. This is the form of the amplitudes that we can expect from Eq. (12.39) and that we will find in the examples in the next section.

Since we want to compute the pseudo-tensor of Landau–Lifshitz, we need to compute the Christoffel symbols of the metric of the spacetime $g_{\mu\nu} = \eta_{\mu\nu} + h^{\mathrm{TT}}_{\mu\nu}$. The only time varying metric coefficients are g_{xx} and g_{yy} and they only depend on the coordinates t and z. The derivatives of h_+ with respect to t and z are, respectively,

$$\begin{aligned} \frac{\partial h_+}{\partial t} &= \frac{C\dot{f}}{z}\,, \\ \frac{\partial h_+}{\partial z} &= -\frac{Cf}{z^2} - \frac{C\dot{f}}{cz} = -\frac{Cf}{z^2} - \frac{1}{c}\frac{\partial h_+}{\partial t}\,. \end{aligned} \tag{12.61}$$

In what follows, we will only consider the leading order term proportional to $1/z$ and we will ignore the contribution proportional to $1/z^2$. The non-vanishing Christoffel symbols are

$$\begin{aligned} &\Gamma^0_{xx} = -\Gamma^0_{yy} = \Gamma^x_{0x} = \Gamma^x_{x0} = -\Gamma^y_{0y} = -\Gamma^y_{y0} = \frac{1}{2}\dot{h}_+\,, \\ &\Gamma^z_{xx} = -\Gamma^z_{yy} = \frac{1}{2c}\dot{h}_+\,, \\ &\Gamma^x_{xz} = \Gamma^x_{zx} = -\Gamma^y_{yz} = -\Gamma^y_{zy} = -\frac{1}{2c}\dot{h}_+\,. \end{aligned} \tag{12.62}$$

After tedious but straightforward calculations, we find the expression of t^{0z}

$$t^{0z} = \frac{c^2}{16\pi G_{\mathrm{N}}}\dot{h}_+^2\,. \tag{12.63}$$

ct^{0z} is the energy flux measured by the distant observer, namely the energy per unit time and unit surface flowing orthogonal to the z axis

$$ct^{0z} = \frac{dE_{\rm GW}}{dt\,dS} = \frac{c^3}{16\pi G_{\rm N}}\dot{h}_+^2 \,. \tag{12.64}$$

If we assume that both polarizations are present and we repeat the calculations, we would find that the energy flux is given by

$$ct^{0z} = \frac{c^3}{16\pi G_{\rm N}}\left(\dot{h}_+^2 + \dot{h}_\times^2\right) = \frac{c^3}{32\pi G_{\rm N}}\sum_{ij}\left(\dot{h}_{ij}^{\rm TT}\right)^2 \,. \tag{12.65}$$

Since in general relativity we cannot provide a local definition of the energy of the gravitational field, it is more correct to rewrite Eq. (12.65) averaging over several wavelengths

$$\frac{dE_{\rm GW}}{dt\,dS} = \langle ct^{0z}\rangle = \frac{c^3}{32\pi G_{\rm N}}\langle\sum_{ij}\left(\dot{h}_{ij}^{\rm TT}\right)^2\rangle \,. \tag{12.66}$$

Let us now write the gravitational wave luminosity in terms of the quadrupole moment of the emitting source. From Eq. (12.55) we can write

$$\begin{aligned}\frac{dE_{\rm GW}}{dt\,dS} &= \frac{G_{\rm N}}{8\pi c^5 r^2}\langle\sum_{ij}\left[\dddot{Q}_{ij}^{\rm TT}\,(t-r/c)\right]^2\rangle \\ &= \frac{G_{\rm N}}{8\pi c^5 r^2}\langle\sum_{ij}\left[P_{ijkl}\ddot{Q}_{kl}\,(t-r/c)\right]^2\rangle\end{aligned} \tag{12.67}$$

The luminosity of the source can be obtained by integrating over the whole solid angle

$$\begin{aligned}L_{\rm GW} &= \frac{dE_{\rm GW}}{dt} = \int\frac{dE_{\rm GW}}{dt\,dS}dS = \int\frac{dE_{\rm GW}}{dt\,dS}r^2\,d\Omega \\ &= \frac{G_{\rm N}}{8\pi c^5}\int d\Omega\,\langle\sum_{ij}\left[P_{ijkl}\ddot{Q}_{kl}\,(t-r/c)\right]^2\rangle \\ &= \frac{G_{\rm N}}{8\pi c^5}\int d\Omega\,\langle\sum_{ij}\left[P_{ijkl}\dddot{\tilde{Q}}_{kl}\,(t-r/c)\right]^2\rangle \,,\end{aligned} \tag{12.68}$$

where $d\Omega$ is the infinitesimal solid angle and in the last passage we have replaced the quadrupole moment with the reduced quadrupole moment because it is more convenient for the next calculations. Remember that Q_{ij} and $\tilde{Q}_{ij}$ only differ by the trace, which is projected out by P_{ijkl}.

To compute the integral over the solid angle, first we rewrite the expression inside the integral as follows

$$\sum_{ij}\left(P_{ijkl}\dddot{\tilde{Q}}_{kl}\right)^2 = \sum_{ij}\left(P_{ijkl}\dddot{\tilde{Q}}_{kl}\right)\left(P_{ijmn}\dddot{\tilde{Q}}_{mn}\right)$$
$$= \sum_{ij}\left(P_{ijkl}P_{ijmn}\dddot{\tilde{Q}}_{kl}\dddot{\tilde{Q}}_{mn}\right) = P_{klmn}\dddot{\tilde{Q}}_{kl}\dddot{\tilde{Q}}_{mn}$$
$$= \Big[\left(\delta_{km}-n_kn_m\right)\left(\delta_{ln}-n_ln_n\right)$$
$$-\frac{1}{2}\left(\delta_{kl}-n_kn_l\right)\left(\delta_{mn}-n_mn_n\right)\Big]\dddot{\tilde{Q}}_{kl}\dddot{\tilde{Q}}_{mn}\,. \quad (12.69)$$

Since $\tilde{Q}_{ij}$ is traceless and symmetric, we have

$$\delta_{kl}\dddot{\tilde{Q}}_{kl} = \delta_{mn}\dddot{\tilde{Q}}_{mn} = 0\,,$$
$$n_kn_m\delta_{ln}\dddot{\tilde{Q}}_{kl}\dddot{\tilde{Q}}_{mn} = n_ln_n\delta_{km}\dddot{\tilde{Q}}_{kl}\dddot{\tilde{Q}}_{mn}\,, \quad (12.70)$$

and Eq. (12.69) becomes

$$\sum_{ij}\left(P_{ijkl}\dddot{\tilde{Q}}_{kl}\right)^2 = \dddot{\tilde{Q}}_{lm}\dddot{\tilde{Q}}_{lm} - 2n_ln_n\dddot{\tilde{Q}}_{lm}\dddot{\tilde{Q}}_{mn} + \frac{1}{2}n_kn_ln_mn_n\dddot{\tilde{Q}}_{kl}\dddot{\tilde{Q}}_{mn}\,. \quad (12.71)$$

The expression for the luminosity of the source now reads

$$L_{\rm GW} = \frac{G_{\rm N}}{8\pi c^5}\int d\Omega\left(\ddot{\tilde{Q}}_{lm}\ddot{\tilde{Q}}_{lm} - 2n_ln_n\ddot{\tilde{Q}}_{lm}\ddot{\tilde{Q}}_{mn} + \frac{1}{2}n_kn_ln_mn_n\ddot{\tilde{Q}}_{kl}\ddot{\tilde{Q}}_{mn}\right), \quad (12.72)$$

and we have to evaluate the following integrals

$$\int d\Omega\, n_in_j\,, \quad \int d\Omega\, n_in_jn_kn_l\,. \quad (12.73)$$

The unit vector $\mathbf{n}$ is

$$\mathbf{n} = (\sin\theta\cos\phi, \sin\theta\sin\phi, \cos\theta)\,. \quad (12.74)$$

It is easy to see that, for $i \neq j$, we have

$$\int d\Omega\, n_in_j = \int_0^\pi d\theta\sin\theta\int_0^{2\pi} d\phi\, n_in_j = 0\,, \quad (12.75)$$

while, for $i = j$, we find

$$\int d\Omega n_x^2 = \int d\Omega n_y^2 = \int d\Omega n_z^2 = \frac{4\pi}{3}\,. \quad (12.76)$$

The first integral in Eq. (12.73) can be written in the following compact form

$$\frac{1}{4\pi}\int d\Omega\, n_i n_j = \frac{1}{3}\delta_{ij}\,. \tag{12.77}$$

We can proceed in a similar way and evaluate the second integral in Eq. (12.73). It turns out that

$$\frac{1}{4\pi}\int d\Omega\, n_i n_j n_k n_l = \frac{1}{15}\left(\delta_{ij}\delta_{kl}+\delta_{ik}\delta_{jl}+\delta_{il}\delta_{jk}\right)\,. \tag{12.78}$$

We put together all the results found in this section and we obtain the total luminosity (or power) of the source in the form of gravitational radiation

$$L_{\rm GW} = \frac{G_{\rm N}}{5c^5}\langle \dddot{\tilde{Q}}_{ij}\,(t-r/c)\cdot \dddot{\tilde{Q}}_{ij}\,(t-r/c)\rangle\,. \tag{12.79}$$

12.5 Examples

Let us now calculate the gravitational waves emitted by two simple systems: (i) a rotating compact object (we can think about a neutron star) which is not perfectly axisymmetric, and (ii) a binary system in circular orbit far from coalescence.

12.5.1 Gravitational Waves from a Rotating Neutron Star

Let us approximate a non-rotating neutron star with an ellipsoid of uniform mass density ρ. The quadrupole moment of the neutron star is

$$Q_{ij} = \int_V \rho x_i x_j\, d^3x\,, \tag{12.80}$$

where V is the volume of the body. The inertia tensor of the neutron star is

$$I_{ij} = \int_V \rho\left(r^2\delta_{ij}-x_i x_j\right)\, d^3x\,, \tag{12.81}$$

and is related to the quadrupole moment by the equation

$$I_{ij} = \delta_{ij}\,Q - Q_{ij}\,. \tag{12.82}$$

The reduced quadrupole moment introduced in Eq. (12.57) is

$$\tilde{Q}_{ij} = Q_{ij} - \frac{1}{3}\delta_{ij} Q = -I_{ij} + \frac{1}{3}\delta_{ij} I \,, \tag{12.83}$$

where I is the trace of the inertia tensor.

The inertia tensor of a non-rotating ellipsoid of constant mass density and with semi-axes α, β, and γ (respectively along the x, y, and z axes) is given by

$$||I_{ij}|| = \frac{M}{5} \begin{pmatrix} \beta^2 + \gamma^2 & 0 & 0 \\ 0 & \alpha^2 + \gamma^2 & 0 \\ 0 & 0 & \alpha^2 + \beta^2 \end{pmatrix} = \begin{pmatrix} I_{xx} & 0 & 0 \\ 0 & I_{yy} & 0 \\ 0 & 0 & I_{zz} \end{pmatrix} , \tag{12.84}$$

where M is the mass of the ellipsoid and I_{xx}, I_{yy}, and I_{zz} are the principal moments of inertia.

Let us now assume that the neutron star is rotating about the z axis with angular velocity Ω. To compute the inertia tensor of the rotating ellipsoid, we consider the rotation matrix connecting the co-rotating and the inertial reference frames

$$||R_{ij}|| = \begin{pmatrix} \cos \Omega t & -\sin \Omega t & 0 \\ \sin \Omega t & \cos \Omega t & 0 \\ 0 & 0 & 1 \end{pmatrix} . \tag{12.85}$$

If the inertia tensor in the co-rotating frame is given by Eq. (12.84), that in the inertial reference frame can be obtained with a rotation

$$I_{ij} \to I'_{ij} = R_{ik} R_{jl} I_{kl} = \begin{pmatrix} I'_{xx} & I'_{xy} & 0 \\ I'_{yx} & I'_{yy} & 0 \\ 0 & 0 & I'_{zz} \end{pmatrix} , \tag{12.86}$$

where

$$\begin{aligned} I'_{xx} &= I_{xx} \cos^2 \Omega t + I_{yy} \sin^2 \Omega t \,, \\ I'_{xy} &= -\left(I_{yy} - I_{xx}\right) \sin \Omega t \cos \Omega t \,, \\ I'_{yx} &= I'_{xy} \,, \\ I'_{yy} &= I_{xx} \sin^2 \Omega t + I_{yy} \cos^2 \Omega t \,, \\ I'_{zz} &= I_{zz} \,. \end{aligned} \tag{12.87}$$

We use the trigonometric identity $\cos 2\Omega t = 2 \cos^2 \Omega t - 1$, and we write the reduced quadrupole moment of the rotating neutron star as

$$||\tilde{Q}_{ij}|| = \frac{I_{yy} - I_{xx}}{2} \begin{pmatrix} \cos 2\Omega t & \sin 2\Omega t & 0 \\ \sin 2\Omega t & -\cos 2\Omega t & 0 \\ 0 & 0 & 0 \end{pmatrix} + \text{constant} \,, \tag{12.88}$$

where the constant part can be ignored because the gravitational wave emission involves the time derivative of the quadrupole moment. Note that

$$I_{yy} - I_{xx} = \frac{M}{5}\left(\alpha^2 + \gamma^2\right) - \frac{M}{5}\left(\beta^2 + \gamma^2\right) = \frac{M}{5}\left(\alpha^2 - \beta^2\right) . \tag{12.89}$$

and therefore, if $\alpha = \beta$, the reduced quadrupole moment is constant and there is no emission of gravitational waves. A perfectly axisymmetric object rigidly rotating about its symmetry axis does not emit gravitational waves.

We define the *oblateness* of the ellipsoid, ε, as

$$\varepsilon = 2\frac{\alpha - \beta}{\alpha + \beta} , \tag{12.90}$$

and we have

$$\frac{I_{yy} - I_{xx}}{I_{zz}} = \varepsilon + O(\varepsilon^3) . \tag{12.91}$$

The reduced quadrupole moment now reads

$$||\tilde{Q}_{ij}|| = \frac{\varepsilon I_{zz}}{2}\begin{pmatrix} \cos 2\Omega t & \sin 2\Omega t & 0 \\ \sin 2\Omega t & -\cos 2\Omega t & 0 \\ 0 & 0 & 0 \end{pmatrix} + \text{constant} . \tag{12.92}$$

The trace-reversed perturbation is

$$\tilde{h}_{ij} = \frac{2G_{\mathrm{N}}}{c^4 r}\ddot{Q}_{ij}\left(t - r/c\right) . \tag{12.93}$$

h_{ij}^{TT} can be obtained with the use of the projector operator, as done in Eq. (12.52)

$$h_{ij}^{\mathrm{TT}} = \frac{4G_{\mathrm{N}}}{c^4 r}\varepsilon\Omega^2 I_{zz} P \begin{pmatrix} -\cos\varphi & -\sin\varphi & 0 \\ -\sin\varphi & \cos\varphi & 0 \\ 0 & 0 & 0 \end{pmatrix} , \tag{12.94}$$

where P indicates the transverse-traceless projector and $\varphi = 2\Omega\left(t - r/c\right)$. Note that the frequency of the gravitational wave is twice the rotational frequency of the neutron star. An estimate of the amplitude of the gravitational wave can be obtained by plugging in some reasonable numbers for a neutron star in our Galaxy

$$\frac{4G_{\mathrm{N}}}{c^4 r}\varepsilon\Omega^2 I_{zz} \sim 10^{-25}\left(\frac{10\ \mathrm{kpc}}{r}\right)\left(\frac{\varepsilon}{10^{-7}}\right)\left(\frac{\Omega}{1\ \mathrm{kHz}}\right)^2\left(\frac{I_{zz}}{10^{38}\ \mathrm{kg}\cdot\mathrm{m}^2}\right) . \tag{12.95}$$

Upper bounds on ε have been obtained from the observed slowing down of the period of pulsars under the assumption that it is entirely due to the emission of gravitational waves [8].

The energy released can be evaluated from Eq. (12.79) and turns out to be

$$L_{\mathrm{GW}} = \frac{32 G_{\mathrm{N}}}{5c^5} \varepsilon^2 \Omega^6 I_{zz}^2 \,. \tag{12.96}$$

12.5.2 Gravitational Waves from a Binary System

Let us consider a binary system in circular orbit in Newtonian gravity. We have body 1 with mass m_1, body 2 with mass m_2, and the total mass is $M = m_1 + m_2$. We choose the coordinate system such that the motion is in the xy-plane and that the origin of the coordinate system coincides with the center of mass

$$r_1 m_1 + r_2 m_2 = 0 \,, \tag{12.97}$$

where r_1 and r_2 are the distances from of origin of, respectively, body 1 and body 2 and are given by

$$r_1 = \frac{m_2 R}{M} \,, \quad r_2 = \frac{m_1 R}{M} \,, \tag{12.98}$$

and $R = r_1 + r_2$ is the orbital separation. The orbital frequency Ω follows from Newton's Universal Law of Gravitation

$$\frac{G_{\mathrm{N}} m_1 m_2}{R^2} = m_1 \Omega^2 r_1 = m_1 \Omega^2 \frac{m_2 R}{M} \quad \Rightarrow \quad \Omega = \sqrt{\frac{G_{\mathrm{N}} M}{R^3}} \,. \tag{12.99}$$

The trajectories of body 1 and of body 2 are, respectively,

$$\mathbf{x}_1 = \begin{pmatrix} r_1 \cos \Omega t \\ r_1 \sin \Omega t \\ 0 \end{pmatrix} \,, \quad \mathbf{x}_2 = \begin{pmatrix} -r_2 \cos \Omega t \\ -r_2 \sin \Omega t \\ 0 \end{pmatrix} \,. \tag{12.100}$$

Let us now compute the quadrupole moment of the binary system. The 00-component of the energy-momentum tensor of the system is

$$T^{00} = \sum_{i=1}^{2} m_i c^2 \delta\left(x - x_i\right) \delta\left(y - y_i\right) \delta\left(z\right) \,. \tag{12.101}$$

The xx-component of the quadrupole moment is

$$
\begin{aligned}
Q_{xx} &= \sum_{i=1}^{2} \int_V m_i x^2 \delta\,(x - x_i)\,\delta\,(y - y_i)\,\delta\,(z)\;dx\,dy\,dz \\
&= m_1 x_1^2(t) + m_2 x_2^2(t) = m_1 r_1^2 \cos^2 \Omega t + m_2 r_2^2 \cos^2 \Omega t \\
&= \frac{\mu R^2}{2} \cos 2\Omega t + \text{constant}\,,
\end{aligned}
\tag{12.102}
$$

where $\mu = m_1 m_2 / M$ is the reduced mass of the binary system, in the last passage we have employed the identity $\cos 2\Omega t = 2\cos^2 \Omega t - 1$, and, as before, we can ignore the constant part because we are interested in the emission of gravitational waves. The other components can be computed in a similar way. Eventually we find the following quadrupole moment

$$
||Q_{ij}|| = \frac{\mu R^2}{2} \begin{pmatrix} \cos 2\Omega t & \sin 2\Omega t & 0 \\ \sin 2\Omega t & -\cos 2\Omega t & 0 \\ 0 & 0 & 0 \end{pmatrix} + \text{constant}\,. \tag{12.103}
$$

Let us assume that the observer is along the z axis far from the source. The unit vector normal to the wavefront is $\mathbf{n} = (0, 0, 1)$. The projector P_{ij} is

$$
||P_{ij}|| = ||\delta_{ij} - n_i n_j|| = \begin{pmatrix} 1 & 0 & 0 \\ 0 & 1 & 0 \\ 0 & 0 & 0 \end{pmatrix}\,. \tag{12.104}
$$

With the projector P_{ij}, we construct the transverse-traceless projector P_{ijkl} and we apply it to the quadrupole moment of the system to obtain the quadrupole moment in the TT gauge. The xx-component of the quadrupole moment in the TT gauge is thus

$$
\begin{aligned}
Q_{xx}^{\mathrm{TT}} &= P_{xxij} Q_{ij} = \left(P_{xi} P_{xj} - \frac{1}{2} P_{xx} P_{ij} \right) Q_{ij} \\
&= \left(P_{xx}^2 - \frac{1}{2} P_{xx}^2 \right) Q_{xx} - \frac{1}{2} P_{xx} P_{yy} Q_{yy} \\
&= \frac{1}{2} \left(Q_{xx} - Q_{yy} \right)\,,
\end{aligned}
\tag{12.105}
$$

and we can evaluate the other components in a similar way. Eventually, we find

$$
||Q_{ij}^{\mathrm{TT}}|| = \begin{pmatrix} \frac{1}{2}\left(Q_{xx} - Q_{yy}\right) & Q_{xy} & 0 \\ Q_{xy} & -\frac{1}{2}\left(Q_{xx} - Q_{yy}\right) & 0 \\ 0 & 0 & 0 \end{pmatrix}\,. \tag{12.106}
$$

The metric perturbation is the TT gauge can be written as

$$||h^{\rm TT}_{\mu\nu}|| = \begin{pmatrix} 0 & 0 & 0 & 0 \\ 0 & h_+(t) & h_\times(t) & 0 \\ 0 & h_\times(t) & -h_+(t) & 0 \\ 0 & 0 & 0 & 0 \end{pmatrix} , \tag{12.107}$$

where

$$\begin{aligned} h_+(t) &= \frac{G_{\rm N}}{c^4 z}\frac{d^2}{dt^2}\left(Q_{xx} - Q_{yy}\right) = -\frac{4G_{\rm N}\mu R^2\Omega^2}{c^4 z}\cos\left[2\Omega\,(t - z/c)\right] , \\ h_\times(t) &= \frac{2G_{\rm N}}{c^4 z}\frac{d^2}{dt^2}Q_{xy} = -\frac{4G_{\rm N}\mu R^2\Omega^2}{c^4 z}\sin\left[2\Omega\,(t - z/c)\right] . \end{aligned} \tag{12.108}$$

As in the case of the rotating ellipsoid in the previous subsection, the frequency of the gravitational wave is twice the frequency of the system. Note that in the case of elliptic orbits, we do not have the emission of a monochromatic gravitational wave. We have instead a discrete spectrum in which the frequencies of the gravitational waves are multiple of the orbital frequency Ω.

12.6 Astrophysical Sources

Generally speaking, potential astrophysical sources of gravitational waves are all the astrophysical systems in which the motion of a large amount of matter alters the background metric. Before listing some detected/expected astrophysical sources in this section and discussing how the generated gravitational waves can be observed in the next section, it is convenient to point out a few important differences between electromagnetic radiation and gravitational waves.

1. Unlike electromagnetic radiation, gravitational waves interact only very weakly with matter, which means that they can travel for very long distances almost unaltered.
2. Electromagnetic radiation is typically generated by moving charged particles in the astrophysical source. The photon wavelength is usually much smaller than the size of the source and is determined by the microphysics. Gravitational waves are instead generated by the motion of the astrophysical source itself, and therefore the emitted radiation has a wavelength comparable to (or larger than) the size of the source.
3. The amplitude of a gravitational wave scales with distance as $1/r$, while electromagnetic signals scale as $1/r^2$. For instance, this implies that, if we double the sensitivity of a gravitational wave detector, we double the distance to which sources can be detected, and we thus increase the number of detectable sources by a factor of 8.

As we have already pointed out, the wavelength (and therefore the frequency) of a gravitational wave depends on the size of the source. For a compact source of mass

M and size L, the characteristic frequency is

$$\nu \sim \frac{1}{2\pi}\sqrt{\frac{G_N M}{L^3}}\,. \tag{12.109}$$

Since the size of the source cannot be smaller than its gravitational radius, i.e. $L > G_N M/c^2$, we find the following upper bound for the frequency of a compact source

$$\nu < \frac{1}{2\pi}\frac{c^3}{G_N M} \sim 10\left(\frac{M_\odot}{M}\right)\ \text{kHz}\,. \tag{12.110}$$

Compact sources can generate high frequency gravitational waves only if they have a small mass. Very heavy systems inevitably produce low frequency gravitational waves.

12.6.1 Coalescing Black Holes

Coalescing black holes are among the leading candidate sources for detection by present and future gravitational wave observatories. Ground-based laser interferometers can detect gravitational waves in the frequency range 10 Hz–10 kHz and consequently can observe the last stage of the coalescence of stellar-mass black holes. Gravitational wave experiments sensitive at lower frequencies can detect signals from the coalescence of two supermassive black holes or from a system of a supermassive black hole and a stellar-mass compact object.

The first direct detection of gravitational waves was in September 2015 [1]. The event was called GW150914 and was the coalescence of two black holes with a mass, respectively, of $36 \pm 5\ M_\odot$ and $29 \pm 4\ M_\odot$. The merger produced a black hole with a mass $62 \pm 4\ M_\odot$, while $3.0 \pm 0.5\ M_\odot$ was radiated in the form of gravitational waves.

The coalescence of a system of two black holes is characterized by three stages (see Fig. 12.3):

1. *Inspiral*. The two objects rotate around each other. This causes the emission of gravitational waves. As the system loses energy and angular momentum, the separation between the two objects decreases and their relative velocity increases. The frequency and the amplitude of the gravitational waves increase (leading to the so-called "chirping" characteristic in the waveform) until the moment of merger.
2. *Merger*. The two black holes merge into a single black hole.
3. *Ringdown*. The newly born black hole emits gravitational waves to settle down to an equilibrium configuration.

Because of the complexity of the Einstein equations, it is necessary to employ certain approximation methods to compute the gravitational wave signal. In the case

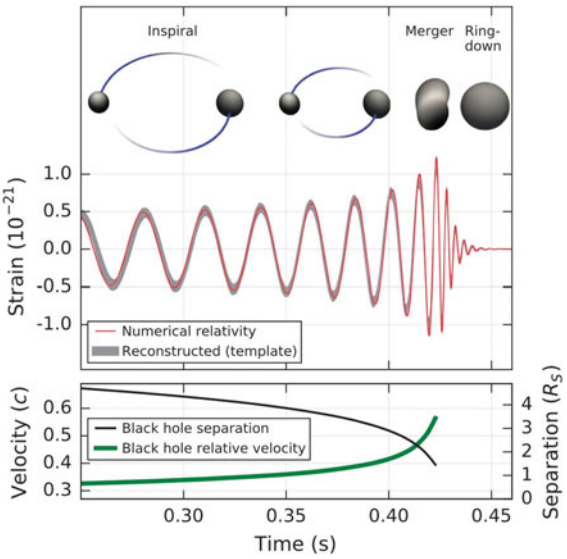

Fig. 12.3 Temporal evolution of the strain, of the black hole separation, and of the black hole relative velocity in the event GW150914 (see Sect. 12.7 for the definition of strain). From [1] under the terms of the Creative Commons Attribution 3.0 License

of (roughly) equal mass black holes, the three stages above are treated with the following methods:

1. *Post-Newtonian (PN) methods*. They are based on an expansion in $\varepsilon \sim U/c^2 \sim v^2/c^2$, where $U \sim G_{\rm N}M/R$ is the Newtonian gravitational potential and v is the black hole relative velocity. The 0PN term is the Newtonian solution of the binary system. The nPN term is the $O(\varepsilon^n)$ correction to the Newtonian solution. In Einstein's gravity, radiation backreaction shows up at 3.5PN order in g_{00}, at 3PN order in g_{0i}, and at 2.5PN order in g_{ij}.
2. *Numerical relativity*. When the PN approach breaks down because ε is not a small parameter any longer, one has to solve numerically the field equations of the complete theory. Since the spacetime is not resolved to infinite precision, even this approach is an approximate method. For non-spinning black holes, the stage of merger smoothly connects the stages of inspiral and of ringdown. For spinning black holes, merger may be a more violent event, depending on the black hole spins and their alignments with respect to the orbital angular momentum.
3. *Black hole perturbation theory*. It is based on the study of small perturbations over a background metric. The method is used to describe the ringdown stage.

12.6.2 Extreme-Mass Ratio Inspirals

An extreme-mass ratio inspiral is a system of a stellar-mass compact object (black hole, neutron star, or white dwarf with a mass $\mu \sim 1$–$10\,M_\odot$) orbiting a supermassive black hole ($M \sim 10^6$–$10^{10}\,M_\odot$). Since the system emits gravitational waves, the

stellar-mass compact object slowly inspirals into the supermassive black hole until the final plunge. A similar system can easily form by multi-body interactions in galactic centers. Initially, the captured object is in a "generic" orbit, namely the orbit will have a high eccentricity and any inclination angle with respect to the black hole spin. Due to the emission of gravitational waves, the eccentricity tends to decreases (if we are far from the last stable orbit), while the inclination of the orbit remains approximately constant [4, 7].

Extreme-mass ratio inspirals are an important class of detection candidates for future space-based gravitational wave interferometers. Detection will be dominated by sources in which the stellar-mass compact object is a black hole rather than a neutron star or a white dwarf. There are two reasons. First, the heaviest bodies tend to concentrate at the center. Second, the signal produced by a 10 $M_\odot$ black hole is stronger than the signal from a neutron star or a white dwarf with a mass $\mu \approx 1\ M_\odot$.

In the frequency range 1–100 mHz, it is possible to detect the last few years of inspiral into a supermassive black hole of $\sim 10^6\ M_\odot$. If the supermassive object is heavier or the inspiral is at an earlier stage, the emission of gravitational waves is at lower frequencies.

Since $\mu/M < 10^{-5}$, the evolution of the system is adiabatic; that is, the orbital parameters evolve on a timescale much longer than the orbital period of the stellar-mass compact object. A rough estimate can be obtained as follows [5]. If we are far from the last stable orbit, the orbital period is

$$T \sim 8\left(1-e^2\right)^{-3/2}\left(\frac{M}{10^6\ M_\odot}\right)\left(\frac{p}{6M}\right)^{3/2}\min\,, \tag{12.111}$$

where p is the semi-latus rectum of the orbit and e is the eccentricity. The timescale of the radiation back-reaction can be estimated as $T_{\rm R} \sim -p/\dot{p}$ and we find

$$T_{\rm R} \sim 100\left(1-e^2\right)^{-3/2}\left(\frac{M}{\mu}\right)\left(\frac{M}{10^6\ M_\odot}\right)\left(\frac{p}{6M}\right)^{4}\min\,. \tag{12.112}$$

As long as $M/\mu \gg 1$, we have $T_{\rm R} \gg T$ and the evolution of the system is adiabatic. This simplifies the description, as we can neglect the radiation back-reaction and assume that the small object follows the geodesics of the spacetime. Extreme-mass ratio inspirals are thus relatively simple systems and offer a unique opportunity to map the metric around supermassive black holes [3, 6, 12]. Since the value of μ/M is so low, the inspiral process is slow, and it is possible to observe the signal for many ($>10^5$) cycles. In such a case, the signal-to-noise ratio can be high and it is possible to accurately measure the parameters of the system. In particular, extreme-mass ratio inspiral detections promise to provide unprecedented accurate measurements of the mass and the spin of supermassive black holes [2].

12.6.3 Neutron Stars

Even compact binary systems with neutron stars (i.e. neutron star-neutron star or neutron star-black hole) are promising candidate sources for ground-based laser interferometers. Since the mass of a neutron star cannot be more than 2–3 $M_\odot$, such binaries generate gravitational waves with an amplitude smaller than those emitted by binaries in which both bodies are black holes. This, in turn, makes their detection more difficult and explains why the first detections of gravitational waves are associated with binary systems in which both objects are black holes.

The coalescence of a system in which at least one of the bodies is a neutron star is still characterized by the three stages discussed in Sect. 12.6.1; that is, inspiral, merger, and ringdown. However, in the presence of a neutron star there are some additional complications because we do not have a purely gravitational system, and also the equation of state of the matter the neutron star is made of can have an impact on the gravitational wave signal.

Isolated neutron stars can also be sources of gravitational waves, for instance after the formation of the neutron star (as in the case of black holes, we could observe the stage of ringdown, and the body emits gravitational waves to settle down to an equilibrium configuration), because of the neutron star rotation and in the presence of deviations from a perfect axisymmetry of the body (see the example discussed in Sect. 12.5.1), or for various stellar oscillation modes and core superfluid turbulences. In principle, the detection of gravitational waves from these systems can be also exploited to study the matter equation of state at super-nuclear densities, which is not possible to do in laboratories on Earth.

12.7 Gravitational Wave Detectors

As we have seen in Sect. 12.2.2 and as illustrated in Fig. 12.2, the passage of a gravitational wave has the effect of altering the proper distances among the particles of a certain system. Gravitational wave detectors can reveal the passage of a gravitational wave by monitoring, in different ways, the proper distance of test-bodies. If the proper distance of two test-bodies is L in flat spacetime and the passage of a gravitational wave causes a variation ΔL, we call the *strain* $h = \Delta L/L$. The strain is the quantity measured by the detector, is related to the amplitude of the gravitational wave, and depends on the orientation of the detector with respect to the propagation direction and on the polarization of the gravitational wave.

Direct detection of gravitational waves is very challenging. This is because the expected amplitude of gravitational waves passing through Earth is extremely small, with h of order 10^{-20}. If r is the distance of the source from the detection point, $h \propto 1/r$. To have a simple idea of the technological difficulties to detect gravitational waves, we can consider that the Earth's radius $R \approx 6,000$ km would change by

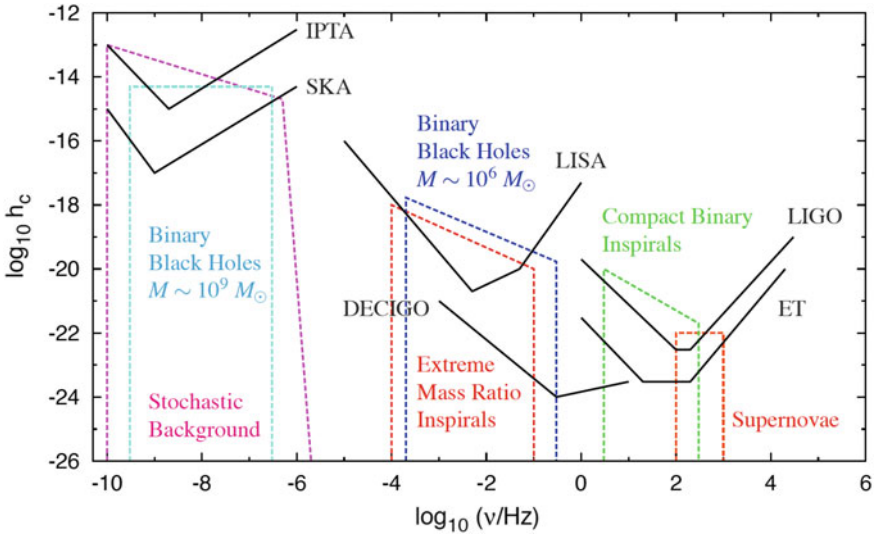

Fig. 12.4 Sketch of the sensitivity curves of a selection of present and proposed gravitational wave detectors in terms of the characteristic strain h_c and of the gravitational wave frequency ν. Resonance spikes in the detector noise curves have been removed for clarity. The figure also shows the expected characteristic strain and frequency of a number of possible astrophysical and cosmological sources

$\Delta R = 60$ fm (1 fm $= 10^{-15}$ m) because of the passage of a gravitational wave with $h = 10^{-20}$. Such a value of ΔR is much smaller than the radius of an atom ($\sim 10^5$ fm).

Table 12.1 lists a selection of recent, present, and future/proposed gravitational wave detectors. There are three main types of detectors, which will be briefly reviewed in the next sections: resonant detectors, interferometers (either ground-based or space-based), and pulsar timing arrays.

Figure 12.4 illustrates the sensitivity curves of a selection of present and proposed gravitational wave detectors together with the expected strength of some gravitational wave sources. In the x-axis, ν is the gravitational wave frequency. The y-axis is for the *characteristic strain* h_c, which is defined as [11]

$$|h_c(\nu)|^2 = 4\nu^2 |\tilde{h}(\nu)|^2 \,, \tag{12.113}$$

where $\tilde{h}(\nu)$ is the Fourier transform of the strain $h(t)$. h_c is not directly related to the amplitude of the gravitational wave, as it includes the effect of integrating an inspiralling signal.

Table 12.1 Partial list of gravitational wave detectors. RD = resonant detector; GBLI = ground-based laser interferometer; SBLI = space-based laser interferometer. Notes: [1] While there may not be an official end of the experiment, resonant detectors are not operative any longer. [2]Expected/proposed

Project	Activity period	Location	Detector type	Frequency range
EXPLORER http://www.roma1.infn.it/rog/explorer/	1990–2002	Geneva (Switzerland)	RD	~900 Hz
ALLEGRO	1991–2008	Baton Rouge (Louisiana)	RD	~900 Hz
NAUTILUS http://www.roma1.infn.it/rog/nautilus/	1995–2002	Frascati (Italy)	RD	~900 Hz
TAMA 300 http://tamago.mtk.nao.ac.jp/spacetime/tama300_e.html	1995–	Mitaka (Japan)	GBLI	10 Hz–10 kHz
GEO 600 http://www.geo600.org	2001–	Sarstedt (Germany)	GBLI	50 Hz–1.5 kHz
AURIGA http://www.auriga.lnl.infn.it	1997–x[1]	Padua (Italy)	RD	~900 Hz
Gravitational Radiation Antenna in Leiden (MiniGRAIL) http://www.minigrail.nl	2001–x[1]	Leiden (Netherland)	RD	2–4 kHz
Laser Interferometer Gravitational Wave Observatory (LIGO) http://www.ligo.org	2004–	Hanford (Washington) Livingston (Louisiana)	GBLI	30 Hz–7 kHz
Mario Schenberg	2006–x[1]	Sao Paulo (Brazil)	RD	3.0–3.4 kHz
Virgo Interferometer http://www.virgo-gw.eu	2007–	Cascina (Italy)	GBLI	10 Hz–10 kHz
Kamioka Gravitational Wave Detector (KAGRA) http://gwcenter.icrr.u-tokyo.ac.jp/en/	From 2018[2]	Kamioka mine (Japan)	GBLI	10 Hz–10 kHz

(continued)

Table 12.1 (continued)

Project	Activity period	Location	Detector type	Frequency range
Indian Initiative in Gravitational Wave Observations (IndiGO) http://gw-indigo.org/tiki-index.php	From 2023[2]	India	GBLI	30 Hz–7 kHz
Deci-hertz Interferometer Gravitational Wave Observatory (DECIGO) http://tamago.mtk.nao.ac.jp/decigo/index_E.html	From 2027[2]	Space	SBLI	1 mHz–10 Hz
Einstein Telescope (ET) http://www.et-gw.eu	From ∼2030[2]	To be decided	GBLI	1 Hz–10 kHz
Laser Interferometer Space Antenna (LISA) https://www.lisamission.org	From 2034[2]	Space	SBLI	0.1 mHz–1 Hz
TianQin	From ∼2040[2]	Space	SBLI	0.1–100 mHz

12.7.1 Resonant Detectors

In the case of resonant detectors, we have a large resonant body (bar) which is stretched and squeezed by the passage of a gravitational wave. The sensitivity of the detector is peaked at its mechanical resonance, which corresponds to the first longitudinal mode of the bar and in most detectors is around 1 kHz. Experiments with resonant detectors quit in the early 2010s because they were not competitive any longer with respect to interferometer detectors.

The first gravitational wave detector was the resonant detector constructed by Joseph Weber in the 1960s. While the claim of a detection of gravitational waves was reported in [14], the sensitivity of that detector was not good enough to detect gravitational waves from astrophysical sources and there is a common consensus on the fact that the claim in [14] was not a real detection.

EXPLORER, ALLEGRO, NAUTILUS, and AURIGA were all cylindrical bar detectors and worked in a similar way. The detector was a heavy bar cooled down to very low temperatures to reduce the thermal noise, namely the motion of the atoms of the bar. The bar was inside vacuum chambers to reduce the acoustic noise of the laboratory. The vibration of the bar was read out by a smaller mass (resonant transducer) of about 1 kg. The transducer had the same resonant frequency as the bar, so it could resonantly pick up the bar vibrations. Since it was much lighter, the amplitude of its vibrations could be much larger.

MiniGRAIL and Mario Schenberg were instead spherical detectors. Spherical antennas are technologically more challenging, but they present some advantages in the possibility of detecting gravitational waves. In particular, a spherical detector can detect gravitational waves arriving from any direction.

12.7.2 Interferometers

Gravitational wave laser interferometers are based on a Michelson interferometer. The set-up of the advanced LIGO detectors is sketched in Fig. 12.5. There are two arms, which are orthogonal to each other. A beamsplitter splits the original laser beam into two beams, which are reflected by the two mirrors at the end of the two arms and eventually recombine and produce an interference pattern. In general, the passage of a gravitational wave would change the travel time in the two arms in a different way: depending on the propagation direction of the gravitational wave with respect to the orientation of the interferometer, one of the arms can be stretched, while the other can be squeezed. The photodetector at the location of the interference pattern can measure a change in the proper length of the arms. To increase the effective path length of the laser light in the arms, there are partially reflecting mirrors, which make the laser light run along the arms many (typically hundreds) times.

TAMA 300 was the first laser interferometer to work, but its sensitivity is limited by its small size. The length of its arms is 300 m. GEO 600 is a laser interferometer

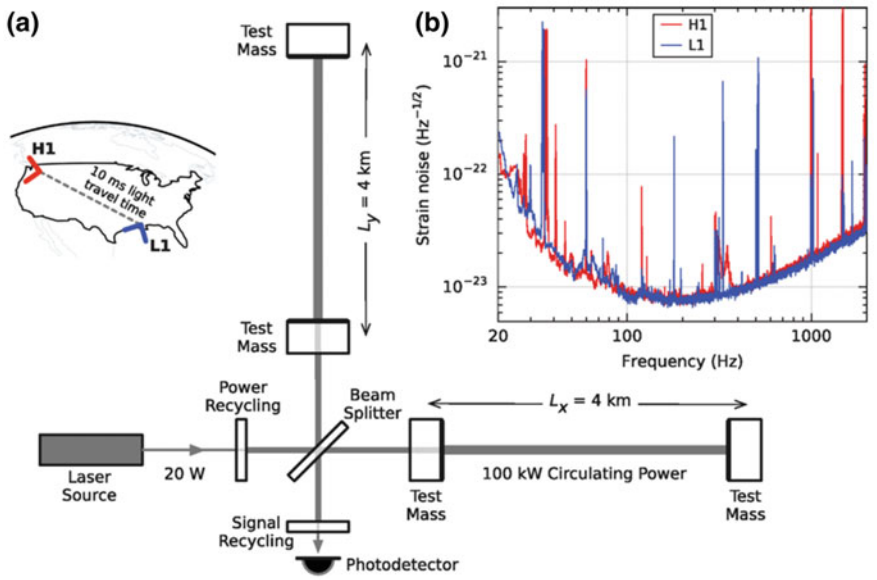

Fig. 12.5 Sketch of the advanced LIGO detectors, location and orientation of the LIGO detectors at Hanford (H1) and Livingston (L1) (**a**), and sensitivity curves in terms of equivalent gravitational wave strain amplitude (**b**). From [1] under the terms of the Creative Commons Attribution 3.0 License

with arms of 600 m. In the case of LIGO and Virgo, the length of the arms is, respectively, 4 and 3 km. Figure 12.6 shows the aerial view of the Virgo detector, near Pisa, in Italy. KAGRA and the Einstein Telescope are underground detectors, to reduce the seismic noise. The Einstein Telescope will have an equilateral triangle geometry, with three arms of 10 km and two detectors at each corner.

Space-based laser interferometers work with a constellation of satellites (e.g. three satellites in LISA and four clusters of three satellites in the case of DECIGO). The working principle is the same as the ground-based laser interferometers, and one wants to monitor the proper distance among mirrors located in different satellites. The distance between satellites is larger than the length of the arms of ground-based laser interferometers, so these experiments are sensitive to gravitational waves at lower frequencies (see Fig. 12.4). This is also possible because the limitation at low frequencies in ground-based experiments is due to seismic noise, but there is no seismic noise in space. In the case of DECIGO, the distance among the satellites should be $\sim 10^3$ km, while the arms of LISA should be $\sim 10^6$ km.

The sensitivity achievable by a laser interferometer can be understood as follows. We can consider the case of LIGO, where the laser wavelength is $\lambda \sim 1\ \mu$m and the interferometer arms have $L = 4$ km. If we could measure ΔL only with a precision of order the size of a fringe, i.e. $\Delta L \sim \lambda$, the minimum detectable strain would be $h \sim \lambda/L \sim 3 \cdot 10^{-10}$. Gravitational waves with a strain of order 10^{-20} can be

Fig. 12.6 Aerial view of the interferometer detector Virgo (Cascina, Pisa, Italy). From the Virgo collaboration under the Creative Commons CC0 1.0 Universal Public Domain Dedication

detected if we can measure changes in the arm length much smaller than λ. The photodetector of the experiment can indeed monitor changes in the photon flux and reach a sensitivity $\Delta L \sim \lambda/\sqrt{N}$, where N is the number of photons arriving at the detector and $\sqrt{N}$ is its fluctuation, being a Poisson process. If P is the laser power, $N \sim P/(\nu E_\gamma)$, where ν is the frequency of the gravitational wave (we can collect photons for a time $t \sim 1/\nu$) and E_γ is the photon energy. If we consider $P \sim 1$ W, $\nu = 100$ Hz, and $\lambda \sim 1$ μm, we find $N \sim 10^{16}$ and $h \sim 10^{-18}$. Moreover, the two arms of the interferometer are two Fabry–Perot optical cavities, and they can store the light for many round trips. For $\nu = 100$ Hz and $L = 4$ km, the light can make about a thousand round trips during the passage of a gravitational wave, which increases the effective arm length by a factor $\sim 10^3$ and the interferometer sensitivity becomes $h \sim 10^{-21}$.

12.7.3 Pulsar Timing Arrays

In a pulsar timing array experiment, the test-bodies are represented by 20–50 ms pulsars. Like in the interferometers of the previous section, the passage of gravitational waves contracts the space in one direction and expands the space in the other direc-

tion, thus changing the arrival time of the pulsar signals on Earth. Since millisecond pulsars can be used as very precise clocks, it is possible to infer variations in the time arrival of the signal of order of some ns.

The distances between Earth and these pulsars in the Galaxy are of the order of 1–10 kpc, which are definitively larger than the distances that we can monitor in interferometric detectors. Pulsar timing array experiments can thus detect gravitational waves of very low frequency, in the range 1–100 nHz. There are two main possible sources for such low frequency gravitational waves. (i) Binary systems of two supermassive black holes with an orbital period ranging from a few months to a few years. Even if they are far from us, the power emitted in gravitational waves is huge, and the signal may be strong enough to be detected. (ii) Gravitational waves produced in the early Universe. There are a number of different scenarios predicting a background of low frequency gravitational waves, like decay of cosmic strings, inflationary models, and first order phase transitions. In all these cases, the frequency of the gravitational waves would be very low because of the cosmological redshift.

At the moment, there are a few operative experiments: the European Pulsar Timing Array (EPTA), the Parkes Pulsar Timing Array (PPTA), the North American Nanohertz Observatory for Gravitational Waves (NANOGrav), and the International Pulsar Timing Array (IPTA). The Square Kilometre Array (SKA) is expected to start in 2020. With the available pulsar data, it is only possible to get some upper bounds on the amplitude of low frequency gravitational waves. These bounds can be improved with time, because the precision is determined by the observational time of the pulsars. We may also discover new millisecond pulsars suitable for these measurements. This would increase the number of sources monitored, which is also helpful to improve the sensitivity.

More details on pulsar timing arrays can be found in [9, 10] and references therein.

Problem

12.1 Derive the estimate of the maximum gravitational wave frequency for black holes with mass $M = 10^6\, M_\odot$ and $10^9\, M_\odot$ from Eq. (12.110) and compare the result with Fig. 12.4.

References

1. B.P. Abbott et al., LIGO scientific and virgo collaborations. Phys. Rev. Lett. **116**, 061102 (2016), arXiv:1602.03837 [gr-qc]
2. L. Barack, C. Cutler, Phys. Rev. D **69**, 082005 (2004). [gr-qc/0310125]
3. L. Barack, C. Cutler, Phys. Rev. D **75**, 042003 (2007). [gr-qc/0612029]
4. J.R. Gair, K. Glampedakis, Phys. Rev. D **73**, 064037 (2006). [gr-qc/0510129]
5. K. Glampedakis, Class. Quant. Grav. **22**, S605 (2005). [gr-qc/0509024]
6. K. Glampedakis, S. Babak, Class. Quant. Grav. **23**, 4167 (2006). [gr-qc/0510057]

7. K. Glampedakis, S.A. Hughes, D. Kennefick, Phys. Rev. D **66**, 064005 (2002). [gr-qc/0205033]
8. E. Gourgoulhon, S. Bonazzola, Gravitational waves from isolated neutron stars, in *Gravitational Waves: Sources and Detectors*, pp. 51–60 (World Scientific, Singapore, 1997). [astro-ph/9605150]
9. G. Hobbs et al., Class. Quant. Grav. **27**, 084013 (2010), arXiv:0911.5206 [astro-ph.SR]
10. A.N. Lommen, Rept. Prog. Phys. **78**, 124901 (2015)
11. C.J. Moore, R.H. Cole, C.P.L. Berry, Class. Quant. Grav. **32**, 015014 (2015), arXiv:1408.0740 [gr-qc]
12. F.D. Ryan, Phys. Rev. D **52**, 5707 (1995)
13. J.M. Weisberg, Y. Huang, Astrophys. J. **829**, 55 (2016), arXiv:1606.02744 [astro-ph.HE]
14. J. Weber, Phys. Rev. Lett. **22**, 1320 (1969)